Check for updates

Strain analysis from M-edge resonant inelastic X-ray scattering of nickel oxide films

P. S. Miedema, [ID] *[a] N. Thielemann-Kühn, [ID] †[bc] I. Alonso Calafell, [ID] ‡[b]
C. Schüßler-Langeheine [ID] [b] and M. Beye [ID] [a]

Electronic structure modifications due to strain are an effective method for tailoring nano-scale functional materials. Demonstrated on nickel oxide (NiO) thin films, Resonant Inelastic X-ray Scattering (RIXS) at the transition-metal $M_{2,3}$-edge is shown to be a powerful tool for measuring the electronic structure modification due to strain in the near-surface region. Analyses from the $M_{2,3}$-edge RIXS in comparison with dedicated crystal field multiplet calculations show distortions in 40 nm NiO grown on a magnesium oxide (MgO) substrate (NiO/MgO) similar to those caused by surface relaxation of bulk NiO. The films of 20 and 10 nm NiO/MgO show slightly larger differences from bulk NiO. Quantitatively, the NiO/MgO samples all are distorted from perfect octahedral (O_h) symmetry with a tetragonal parameter Ds of about -0.1 eV, very close to the Ds distortion from octahedral (O_h) symmetry parameter of -0.11 eV obtained for the surface-near region from a bulk NiO crystal. Comparing the spectra of a 20 nm film of NiO grown on a 20 nm magnetite (Fe_3O_4) film on a MgO substrate (NiO/Fe_3O_4/MgO) with the calculated multiplet analyses, the distortion parameter Ds appears to be closer to zero, showing that the surface-near region of this templated film is less distorted from O_h symmetry than the surface-near region in bulk NiO. Finally, the potential of $M_{2,3}$-edge RIXS for other investigations of strain on electronic structure is discussed.

[a] *Deutsches Elektronen Synchrotron DESY, Notkestraße 85, 22607 Hamburg, Germany. E-mail: p.s.miedema@gmail.com*
[b] *Institute Methods and Instrumentation for Synchrotron Radiation Research (FG-ISRR), Helmholtz-Zentrum Berlin für Materialien und Energie GmbH, Albert-Einstein-Straße 15, 12489 Berlin, Germany*
[c] *Institut für Physik und Astronomie, Universität Potsdam, Karl-Liebknecht-Straße 24/25, 14476 Potsdam, Germany*
† Present address: Fachbereich Physik, Freie Universität Berlin, Arnimallee 14, 14195 Berlin, Germany.
‡ Present address: Vienna Center for Quantum Science and Technology (VCQ), Faculty of Physics, University of Vienna, Boltzmanngasse 5, Vienna A-1090, Austria.

Introduction

The electronic structure of nano-sized layers on surfaces of functional solid materials may be different to that of bulk samples. In particular, epitaxial strain between the nano-layers and substrate surfaces provides a powerful strategy to manipulate (atomic-scale) physical properties by shortening or extending their chemical bonds *via* lattice-mismatch, commonly referred to as strain engineering. This strain engineering has become a key tactic for improving material properties of graphene and similar materials,[1,2] high-T_c superconductors,[3] energy storage materials,[4] quantum materials[5] and solid heterogeneous (electro-)catalysts.[6–10]

Lattice strain is typically measured through the analysis of lattice peak positions measured with hard X-ray diffraction. On nano-sized materials the low amount of material together with

small interaction cross sections for the hard X-ray radiation only provides small signals, averaged over the whole film thickness. Especially for the analysis of strain in surface-near regions, signals are largely shielded by the stronger bulk diffraction. In addition, it is not the lattice changes due to strain themselves that are important in strain engineering, but it is the associated change in electronic structure, *e.g.*, the band gap and valence and conduction band properties, that ultimately leads to enhanced properties of the material. Already for simple binary correlated oxides, *e.g.*, cobalt(II) oxide (CoO)[8,11] and nickel oxide (NiO),[12,13] the strain of the system has been shown to have an influence on properties such as the orbital polarization or the spin and corresponding relative magnetization, or on catalytic activity. For more complex materials strain engineering provides an attractive alternative method for tailoring materials' properties beyond what is possible through doping or chemical substitution.[10,14]

As combination of X-ray absorption and emission spectroscopy, Resonant Inelastic X-ray Scattering (RIXS), is specific for determining electronic structure properties such as the band gap,[15] covalent interactions,[16] potential energy surfaces[17] and excited states[18] with element- and oxidation-state specificity. In this report it will be shown that RIXS is also sensitive to changes in electronic structure due to induced strain. Usually for 3d-transition metal materials, Metal $L_{2,3}$-edge RIXS (schematically $2p^6 3d^n \rightarrow 2p^5 3d^{n+1} \rightarrow 2p^6 3d^n$) is performed for bulk electronic structure studies, partially because it turns out to provide the

21596 | *Phys. Chem. Chem. Phys.*, 2019, **21**, 21596–21602

This journal is © the Owner Societies 2019

best possible energy resolution due to sharpest core levels and thus highest chemical and functional information.[19] However, to provide information on the electronic structure near surfaces, $M_{2,3}$-edge RIXS ($3p^6 3d^n \rightarrow 3p^5 3d^{n+1} \rightarrow 3p^6 3d^n$) is a viable alternative. In particular, for heterogeneous solid catalyst systems, the (near-) surface region provides the chemical activity and a detailed understanding of the changes of the electronic structure in this region is crucial. The X-ray attenuation length in (bulk) NiO is much shorter when addressing the $M_{2,3}$ resonances instead of the $L_{2,3}$ levels: across the full $L_{2,3}$-edge resonances an average attenuation length of about 50 nm is observed for NiO, with detuning from the L_3-edge maximum yielding probing depths of around 300 nm. For the $M_{2,3}$-edge the probing depth is roughly 16 nm[20] and thus provides much higher sensitivity to the near-surface region, while $L_{2,3}$-edge RIXS probes a more significant part of the bulk of the sample. Therefore the $M_{2,3}$-edge RIXS of 3d-transition metal materials is particularly well-suited to study the electronic structure changes in thin films induced by strain from the substrate.

In this research, we will provide theoretical Ni M-edge RIXS multiplet calculations with tetragonal distortions from octahedral (O_h) symmetry. We will show that as a function of distortion, certain signals in the RIXS spectra are changing and in particular that ratios between particular peak areas can be used to quantify the distortion from O_h symmetry. As such, the theoretically obtained ratios can be matched onto ratios obtained for experimental spectra of different NiO systems.

Experimental and theoretical section

10, 20 and 40 nm thin films of NiO were grown on single crystalline MgO(001) substrates (NiO/MgO) via molecular beam epitaxy (MBE). The base pressure in the MBE chamber was 10^{-10} mbar. For the sample preparation oxygen (O$_2$) was led into the chamber via a leak valve until the pressure reached 5×10^{-7} mbar. In the O$_2$ atmosphere Ni metal was evaporated from a Knudsen cell with 1 Å min^{-1} onto the substrate resulting

in epitaxial growth of NiO. Epi-polished MgO substrates were cleaned by annealing them in O$_2$ atmosphere at 600 °C. In addition, a 20 nm NiO film was grown on a 20 nm magnetite (Fe$_3$O$_4$) film, which was itself epitaxially grown on MgO (NiO/Fe$_3$O$_4$/MgO). The film thickness was determined with a quartz-balance thickness monitor during growth. The monitor was calibrated against X-ray reflectivity measurements of prepared films. Reflectivity data were also used to check for thickness variation, which were found to be well below one monolayer within the region of the sample. With lattice constants of $a =$ 4.21 Å for MgO(001) and $a = 8.4$ Å for Fe$_3$O$_4$(001), the lattice mismatch for NiO ($a = 4.18$ Å) is 0.72% and 0.48% respectively. A bulk NiO single crystal from MaTeck was cleaved along the (001) direction before transferring it to the RIXS setup.

Nickel $M_{2,3}$-edge RIXS measurements were performed with a predecessor of the SolidFlexRIXS-setup[21] attached to the UE-112/PGM1 beamline[22] at the BESSY-II synchrotron in Berlin, Germany. The Nickel $M_{2,3}$-edge absorption spectra were recorded via sample drain current measurements.[23] The first M_3 resonance maximum occurred at 67.2 eV and was selected as excitation energy for the RIXS experiments, since it is sufficiently below the threshold of the 3p core ionization. The RIXS spectra for the nano-layer NiO-films required acquisition times of typically three to four hours with the used setup, while for the NiO bulk sample a measurement time of only 90 minutes was considered sufficient. The incident X-rays were horizontally polarized in order to reduce the elastic scattering contribution to the RIXS spectra and the samples were rotated with the sample normal around 60° to the incoming beam, resulting in the normal being 30° off the direction of the spectrometer mounted at a right angle to the incoming beam in the horizontal polarization plane.

The Quanty package[24–26] was used to calculate Ni M-edge horizontally polarized X-ray absorption spectra (XAS) and RIXS calculations with horizontal incoming polarization (X in) and the orthogonal outgoing polarizations ($Y + Z$ out), thereby simulating the experimental geometry with the RIXS spectrometer in the plane of the incoming polarization. Simulations
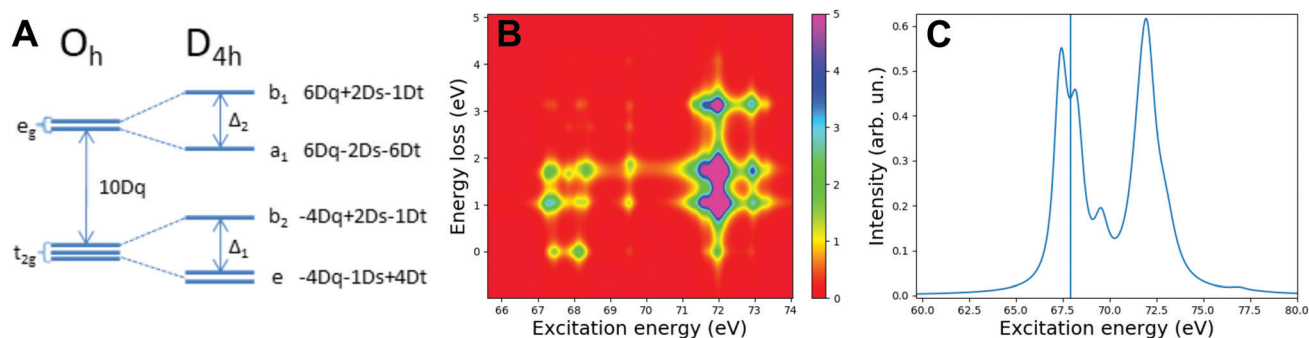
Fig. 1 (A) 3d-Orbital splitting from O_h (left) in a D_{4h}-type symmetry with e (d_{xz}, d_{yz}), b_2 (d_{xy}), a_1 (d_{z^2}) and b_1 ($d_{x^2-y^2}$). One-electron energies due to the (distorted) crystal field splitting are shown as function of Dq, Ds and Dt[27,28] and the splitting due to Δ_1 and Δ_2 is shown as used in the quantity multiplet simulations performed here. (B) Calculated Ni M-edge RIXS with horizontally polarized excitation and emission from the orthogonally polarized components. (C) Calculated Ni M-edge horizontally polarized XAS. For panels B and C the parameters in the multiplet calculations with Ni^{2+} were 10Dq = 1.05, $\Delta_1 = \Delta_2 = 0$ eV and 0.3 eV Gaussian broadening and the excitation energy scale was shifted by 66.8 eV. The vertical line in panel C indicates the excitation energy of the RIXS slices for all calculations with varying Δ_1, Δ_2 (or Ds) used in further analyses.

were performed for Ni^{2+} in octahedral (O_h) symmetry with a crystal field value of $10Dq = +1.05$ eV and with a negligible magnetic field of $H = 0.000001$ T. Distortions from O_h symmetry were taken into account with two parameters called Δ_1 and Δ_2, where Δ_1 splits the original t_{2g} levels and Δ_2 the original e_g levels of the O_h symmetry as shown in Fig. 1A.

The energetic splitting of the d-orbitals can be equivalently formulated with Δ_1 and Δ_2 or with the symmetry parameters Ds and Dt. The one-electron energies as function of Dq, Dt and Ds are shown in Fig. 1A. The Δ_1 and Δ_2 approach can be used to test the behavior of the t_{2g} and e_g splitting independently. In addition, this approach can be used in tests of symmetry distortions that are different from the D_{4h}-type. While ignoring Dt (Dt = 0 eV) to account only for small distortions to octahedral symmetry, for example due to Jahn–Teller distortions, the relationship between Ds and Δ_1 and Δ_2 is: $\Delta_1 = 3 \times$ Ds, $\Delta_2 = 4 \times$ Ds. As for such simulations with Ds distortions, the $\Delta_2 = 4/3 \times \Delta_1$ relationship was fixed.

The simulations for Ni^{2+} with $10Dq = 1.05$ eV and various distortions Ds in eV yield linearly polarized XAS and full RIXS maps. One set is shown in Fig. 1B and C for comparison with the experimental data. RIXS slices were taken at the vertical line indicated in the XAS spectrum of Fig. 1C. We chose a single value for 10Dq, for both ground and X-ray excited state for sake of simplicity, however it is known that 10Dq may be different in the ground state (and RIXS final state) and the X-ray excited state.[29] Overall, the first band in these simulations agreed with the chosen 67.2 eV excitation energy of the experimental data. In addition, the overall calculated XAS shape agreed well with the experimental XAS of bulk NiO.[30]

Results and discussion

Slices from the calculated RIXS maps at the discussed excitation energy (vertical line in Fig. 1C) for a few values of the combined distortion parameters Δ_1 and Δ_2 in (their fixed $\Delta_2 = 4/3 \times \Delta_1$ relationship for) Ds are presented in Fig. 2A. The spectra in Fig. 2A show minor changes in the energetic positions as function of Ds, which would not be detectable within our experimental resolution. There are, however, pronounced changes in the spectral weights of the peaks at ~ 1 eV and 1.76 eV (referred to further as peak 2 and 3 as indicated in Fig. 2B). These peaks can be identified as 3d–3d excitations from the Ni^{2+} $^3A_{2g}$ ground state to $^3T_{2g}$ and $^3T_{1g}$ excited states. Note that the 3d–3d excitation corresponding to the peak around 1 eV is a $t_{2g} \rightarrow e_g$ excitation, so there is a direct relationship of this peak with the 10Dq splitting.

In order to have an analysis of the areas of peak 2 and peak 3 in the simulated spectra that can directly be related to experimental
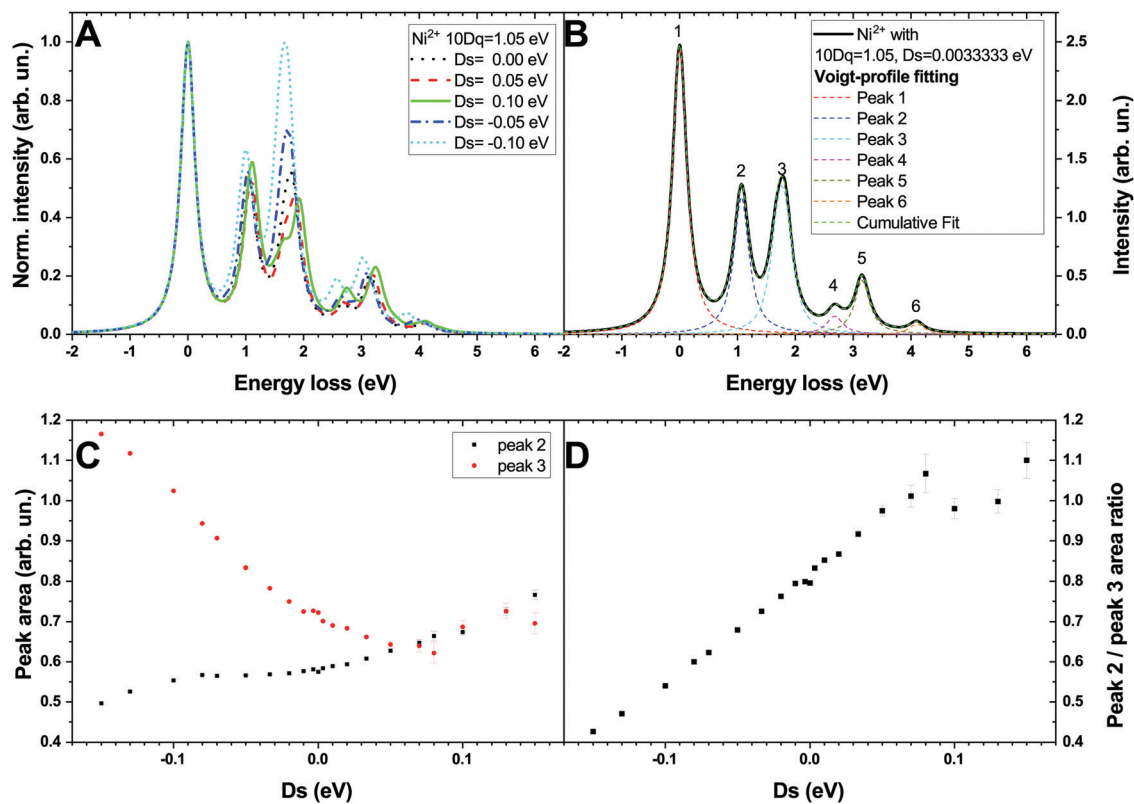

Fig. 2 (A) RIXS slices of multiplet calculations of Ni^{2+} with fixed $10Dq = 1.05$ eV and with several Ds distortions in eV. All spectra in panels A are shown as normalized intensity *versus* energy loss in eV; (B) multi-peak fitting six peaks using Voigt profiles: example for the M-edge RIXS slice of a calculation of Ni^{2+} with $10Dq = 1.05$ and Ds = 0.0033333 eV; (C) peak area analysis from the multi-peak fitting and (D) peak 2/peak 3 area ratio as function of Ds for Ni^{2+} with $10Dq = 1.05$ eV.

21598 | *Phys. Chem. Chem. Phys.*, 2019, **21**, 21596–21602

This journal is © the Owner Societies 2019

data, were fitted six Voigt-profiles to the calculated spectra for a range of Ds-values in between −0.15 and +0.15 eV. An example of this analysis for a $M_{2,3}$-edge RIXS slice of Ni^{2+} with 10Dq = 1.05 and Ds = 0.0033333 eV is shown in Fig. 2B. Fig. 2C summarizes the obtained peak area fitting results for different values of Ds, displaying the trends in spectral weight of peak 2 and 3 as a function of Ds: the peak 2 weight increases, while the peak 3 decreases with increasing Ds. These trends are becoming less clear for Ds ≥ 0.07 eV as will be discussed shortly. The peak 2/peak 3 area ratio as a function of Ds is shown in Fig. 2D, which may be directly compared to the values found for experimental data shown below. The peak area ratio in panel D is roughly linear with the distortion Ds, up to Ds ≈ 0.07 eV. For larger Ds values, the fitting procedure using six peaks begins to deviate from the simulated spectra, since peak 3 starts to split into two components starting around this value of Ds = 0.07 eV (for example, the green solid line with Ds = 0.1 eV in Fig. 2A shows a side-band component in peak 3). For the remaining discussion we restrict ourselves to Ds values where this splitting is small enough to be ignored.

We further mention that the energetic positions of peak 2 and 3, which for both peaks increase slightly with Ds (see e.g., Fig. 2A), yields additional qualitative information about the value and sign of the distortion parameter Ds, especially when symmetry distortions due to strain become large, e.g., when the value of Ds is on the order of Dq (= 10Dq/10).

The experimental Ni $M_{2,3}$-edge XAS of all the investigated samples appear similar to the NiO bulk spectrum measured by Chiuzbăian et al.[30] The 67.2 eV feature was chosen as the excitation energy for our experimental $M_{2,3}$-edge RIXS. The measured RIXS spectra at an excitation energy of 67.2 eV for the different film thicknesses (10, 20 and 40 nm) layers of NiO on MgO (NiO/MgO), as well as a 20 nm film of NiO on a 20 nm film of Fe_3O_4 on MgO (NiO/Fe_3O_4/MgO), and the spectrum from a NiO bulk crystal are shown in Fig. 3A as function of energy loss in eV. Compared to the RIXS spectrum of the NiO bulk

(blue line) in Fig. 3A, the inelastic features at about 1 eV (peak 2) and 1.6–1.7 eV (peak 3) are enhanced for all the nano-layered NiO samples. The elastic line (peak 1) is about 100 to 1000 times higher than the energy loss features and has been cut off for clarity. Due to potential saturation effects in the elastic peak, its shape gets distorted. Therefore the peak analysis was performed as follows: the elastic line (peak 1) is assumed to be perfectly symmetric and the background found at negative energy loss is subtracted from the positive energy loss side before integrating the areas of peaks 2 or peak 3. The peak analysis results for the different samples are displayed in Fig. 3B and C. Both peak 2 and peak 3 areas in Fig. 3B are decreasing as function of increasing nano-layer film size on MgO and are approaching the peak areas obtained for NiO bulk.

The peak ratios of the experimental data in Fig. 3C for the 10, 20, 40 nm NiO/MgO and bulk samples are around 0.5–0.55. Comparing these ratios of the experimental data with the analyses of the Quanty calculations in Fig. 2D suggests negative values of Ds of about −0.10 ± 0.02 eV for all those samples, e.g., the ratios of 0.54, 0.52, 0.52 and 0.50 relate to rounded-off Ds values of −0.10, −0.11, −0.11 and −0.11 eV for the respective 10 nm, 20 nm, 40 nm NiO on MgO and bulk NiO samples. Observing that the sign of Ds is negative is logical, since the lattice constants of the MgO and Fe_3O_4 substrates are larger than the NiO lattice constant. That allows the Ni–O bonds in-plane to extend and in a crystal field description that leads to energy lowering of for example the $3d_{x^2-y^2}$ orbital (b_1 in Fig. 1A) compared to the $3d_{z^2}$ (a_1) orbital. In order to simulate such an effect of a lower relative energy for the b_1 orbital compared to the a_1 orbital, Ds should be negative.

Since the signal in the $M_{2,3}$-edge RIXS experiment is dominated by the topmost 15 nm, the peak area ratios show that the growth of NiO layers on MgO beyond a 20 nm thickness already becomes more bulk-like, e.g., the probed surface-near layers further away from the MgO substrate (e.g., the surface-near region of both the 20 and 40 nm NiO on MgO) are having a
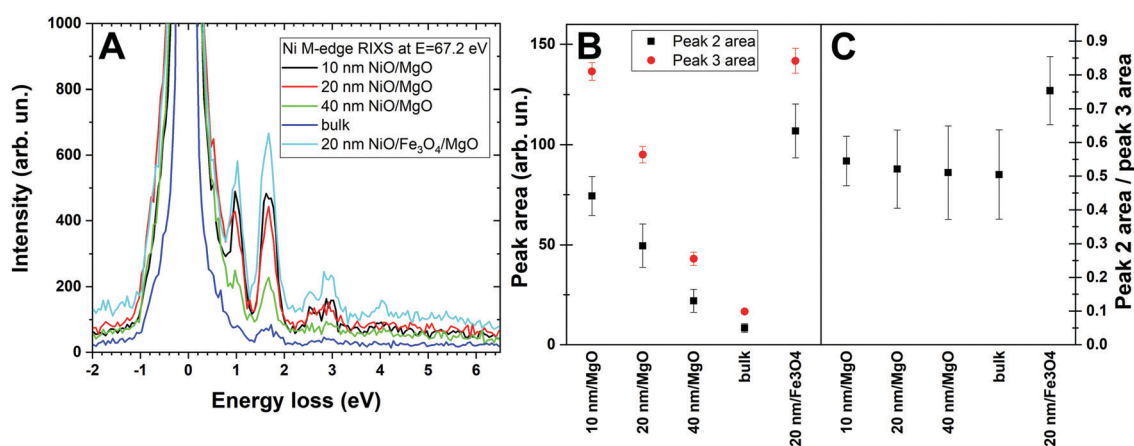

Fig. 3 (A) Ni M-edge RIXS at an incident X-ray energy of 67.2 eV as function of energy loss in eV for NiO bulk (blue), 40 nm NiO/MgO (green), 20 nm NiO/MgO (red), 10 nm NiO/MgO (black) and 20 nm NiO/20 nm Fe_3O_4/MgO (light blue) with the maximum of the elastic line extending up to $2-4 \times 10^5$ a. u. (B) Peak areas of peak 2 (black squares) and 3 (red dots) from area integration of the RIXS spectra for the different NiO/MgO samples and the 20 nm NiO on Fe_3O_4 on MgO (20 nm/Fe_3O_4) compared to NiO bulk. (D) Peak 2/peak 3 area ratio for the different NiO thicknesses on MgO and the 20 nm NiO on 20 nm of Fe_3O_4 on MgO (20 nm/Fe_3O_4) compared to NiO bulk.

This journal is © the Owner Societies 2019

Phys. Chem. Chem. Phys., 2019, **21**, 21596–21602 | **21599**

similar lattice as NiO bulk. Strain effects due to the substrate are expected to decrease with increasing layer thickness, ultimately leading to surfaces that resemble the electronic structure similar of the bulk material. This trend is indeed been found in our M-edge RIXS electronic structure analyses for NiO/MgO, e.g., the average peak area ratio of 10 nm NiO/MgO is different from the NiO bulk, while the average peak area ratio of 40 nm NiO/MgO is already very similar to the NiO bulk, showing the robustness of the M-edge RIXS method for electronic structure characterization due to strain. Taking into account the error bars all nanolayered NiO films on MgO can be considered similar to bulk NiO. (Note that the error bars in Fig. 3C are rather large due to the analysis procedure applied to the experimental data and derives from the noise level of the acquired data.)

Focusing on the experimental analysis obtained for the bulk NiO, the symmetry of bulk NiO is often considered to be Ni^{2+} in an O_h surrounding. However, it is known since the 1940s that crystalline bulk NiO has a small orthorhombic distortion.[31] In addition, in the case of M-edge RIXS, the (near-)surface region of bulk NiO is probed which may be different from the overall bulk NiO as pointed out by Freitag et al.[32] This validates our observation of a substantial distortion from O_h symmetry for bulk NiO.

In order to test the Ni M-edge RIXS procedure to a different induced strain, a 20 nm $NiO/Fe_3O_4/MgO$ was grown and the experimental RIXS spectrum is shown as well in Fig. 3A (light blue line). From the experimental RIXS spectrum of 20 nm $NiO/Fe_3O_4/MgO$ in Fig. 3A, it is already clear that the energy loss peaks 2 and 3 are more intense than for the 20 nm NiO/MgO (Fig. 3B): one easily observes that the peak areas for 20 nm $NiO/Fe_3O_4/MgO$ (marked as 20 nm/Fe_3O_4 on the NiO thickness scale in Fig. 3B) are approximately 1.5–2 times higher than the 20 nm NiO/MgO. The peak 2/peak 3 area ratios in Fig. 3C for 20 nm NiO/MgO and NiO bulk samples compared to the 20 nm $NiO/Fe_3O_4/MgO$ substantiate that the 20 nm $NiO/Fe_3O_4/MgO$ has a different induced strain than the NiO/MgO samples. The 20 nm $NiO/Fe_3O_4/MgO$ has a peak ratio of ~ 0.75 relating to a Ds distortion in the quanty calculations of -0.025 eV, e.g., a value which is much closer to zero than the previously discussed NiO/MgO and bulk NiO samples. As mentioned before, the lattice parameter mismatch of Fe_3O_4 with NiO (0.48%) should be smaller than the mismatch of MgO with NiO (0.72%). Thus, surprisingly, we observed that the obtained Ds distortion of 20 nm $NiO/Fe_3O_4/MgO$ differs more from the bulk NiO than the 20 nm NiO/MgO does. We should point out here that the Fe_3O_4 unit cell has to match two NiO unit cells so that could somewhat explain our unexpected observation. In addition, the fact that Fe_3O_4 grown on MgO also has a lattice mismatch, which might not be compensated yet after 20 nm of Fe_3O_4 layers, needs also to be taken into account. Ultimately this seems to lead to NiO nano-layer growth on top that is more O_h-symmetric than the near-surface crystal structure of a bulk NiO crystal.

For the theoretical analyses shown above, 10Dq = 1.05 eV was fixed agreeing well with the experimental data (peak 2 energy loss position) and published values for NiO.[30] In order

to analyze the robustness of our Ds calibration with respect to the choice of 10Dq, the dependence of the above analyses on different values of 10Dq is checked by varying the distortion Ds for fixed 10Dq = 0.8 and 10Dq = 1.2 eV. For 10Dq = 0.8 eV similar trends as above remain present, although absolute values for the peak ratios are somewhat different. Since 10Dq = 0.8 eV shows the energetic position of peak 2 at 0.8 eV and peak 3 at about 1.6 eV, this 10Dq is considered not to be realistic for matching the experimental data. For a 10Dq value of 1.2 eV, peak 3 generally shows a double structure, which is in disagreement with the experimental data shown in Fig. 3A, so the energetic position and shape of peaks 2 and 3 strongly depend on the choice of 10Dq and agreement with the experiment enforces values 1.05 ± 0.05 eV.

The provided multiplet analyses demonstrate the potential of obtaining lattice distortion related electronic structure information with $M_{2,3}$-edge RIXS. Furthermore we performed M-edge RIXS calculations for other 3d-transition metal ions (e.g., Co^{2+}, Fe^{2+}) and observe clear relationships between distortions of the ligand field around the metal ion and features in the RIXS spectra. Thus, a very similar M-edge analysis procedure for electronic structure modifications could also be used for analysis of, for example, cobalt oxide nano-films.[8,11]

Although the SolidFlexRIXS setup that we used was not set to the optimal resolution in order to improve count rates, we want to stress here that for M-edge RIXS nowadays sub-100 meV resolutions are achieved with rather compact instruments, very much in contrast to $L_{2,3}$-edge RIXS of 3d-transition metal materials, where such energy resolution can only be achieved with huge experimental effort. Also it should be noted that the energy range of the $M_{2,3}$-edges of 3d-transition metal materials can be achieved with lab-high-harmonic-generation (HHG) sources. Although current HHG sources do not provide sufficient flux to perform the here presented RIXS experiments, we expect future developments increasing photon flux in combination with increased efficiency of RIXS optics,[33,34] such that one could foresee that this type of strain engineering analyses with M-edge RIXS may be performed in the lab in the future.

Summary and conclusions

Concluding, strain engineering of thin films by choosing the right combination of substrate and sample material is a key tactic for improving materials' functional properties. In this work we have shown that 3d-transition metal $M_{2,3}$-edge RIXS is a powerful tool for analyzing the electronic structure resulting from the strained 3d-transition metal oxide films on different substrates: experimental Ni $M_{2,3}$-edge RIXS spectra of several nanometer thicknesses of NiO on a substrate and of a bulk NiO crystal were presented and analyzed in terms of the two most intense inelastic features. The experimental results were compared with analyses of RIXS calculations with Ni^{2+} using a fixed crystal field of 10Dq = 1.05 eV in O_h symmetry and on top of that distortions with the Ds parameter leading to splitting of both the e_g and t_{2g} 3d-orbital sets. We observed trends in the analyses

21600 | Phys. Chem. Chem. Phys., 2019, 21, 21596–21602

This journal is © the Owner Societies 2019

from calculated spectra as function of distortion, *e.g.*, the ratio between the areas of the two most intense inelastic features was shown to provide a measurement of the structural distortion Ds and could be used for quantitatively deriving distortions from experimental data.

Conflicts of interest

There are no conflicts to declare.

Acknowledgements

References

1 M. A. Bissett, M. Tsuji and H. Ago, Strain engineering the properties of graphene and other two-dimensional crystals, *Phys. Chem. Chem. Phys.*, 2014, **16**, 11124–11138, DOI: 10.1039/C3CP55443K.

2 S. Deng, A. V. Sumant and V. Berry, Strain engineering in two-dimensional nanomaterials beyond graphene, *Nano Today*, 2018, **22**, 14–35.

3 O. Ivashko, M. Horio, W. Wan, N. B. Christensen, D. E. McNally, E. Paris, Y. Tseng, N. E. Shaik, H. M. Rønnow, H. I. Wei, C. Adamo, C. Lichtensteiger, M. Gibert, M. R. Beasley, K. M. Shen, J. M. Tomczak, T. Schmitt and J. Chang, Engineering the Mott state of cuprates for high-temperature superconductivity, 2018, ArXiv. 1805 (2018) 07173v2. http://arxiv.org/abs/1805.07173.

4 T. Kawaguchi, M. Sakaida, M. Oishi, T. Ichitsubo, K. Fukuda, S. Toyoda and E. Matsubara, Strain-induced stabilization of charged state in Li-rich layered transition metal oxide for lithium ion batteries, *J. Phys. Chem. C*, 2018, **122**, 19298–19308, DOI: 10.1021/acs.jpcc.8b03205.

5 X. Liu, C. F. Chang, A. D. Rata, A. C. Komarek and L. H. Tjeng, Fe$_3$O$_4$ thin films: controlling and manipulating an elusive quantum material, *npj Quantum Mater.*, 2016, **1**, 16027, DOI: 10.1038/npjquantmats.2016.27.

6 M. Luo and S. Guo, Strain-controlled electrocatalysis on multimetallic nanomaterials, *Nat. Rev. Mater.*, 2017, **2**, 17059, DOI: 10.1038/natrevmats.2017.59.

7 K. Amakawa, L. Sun, C. Guo, M. Hävecker, P. Kube, I. E. Wachs, S. Lwin, A. L. Frenkel, A. Patolla, K. Hermann, R. Schlögl and A. Trunschke, How strain affects the reactivity of surface metal oxide catalysts, *Angew. Chem., Int. Ed.*, 2013, **52**, 13553–13557.

8 T. Ling, D. Y. Yan, H. Wang, Y. Jiao, Z. Hu, Y. Zheng, L. Zheng, J. Mao, H. Liu, X. W. Du, M. Jaroniec and S. Z. Qiao, Activating cobalt(II) oxide nanorods for efficient electrocatalysis by strain engineering, *Nat. Commun.*, 2017, **8**, 1509, DOI: 10.1038/s41467-017-01872-y.

9 L. Wang, Z. Zeng, W. Gao, T. Maxson, D. Raciti, M. Giroux, X. Pan, C. Wang and J. Greeley, Tunable intrinsic strain in two-dimensional transition metal electrocatalysts, *Science*, 2019, **363**, 870–874, DOI: 10.1126/science.aat8051.

10 Z. F. Huang, J. Wang, Y. Peng, C. Y. Jung, A. Fisher and X. Wang, Design of efficient bifunctional oxygen reduction/evolution electrocatalyst: recent advances and perspectives, *Adv. Energy Mater.*, 2017, **7**, 1700544, DOI: 10.1002/aenm.201700544.

11 S. I. Csiszar, M. W. Haverkort, Z. Hu, A. Tanaka, H. H. Hsieh, H. J. Lin, C. T. Chen, T. Hibma and L. H. Tjeng, Controlling orbital moment and spin orientation in CoO layers by strain, *Phys. Rev. Lett.*, 2005, **95**, 187205, DOI: 10.1103/PhysRevLett.95.187205.

12 H.-L. Chen, Y.-M. Lu and W.-S. Hwang, Effect of film thickness on structural and electrical properties of sputter-deposited nickel oxide films, *Mater. Trans.*, 2005, **46**, 872–879, DOI: 10.2320/matertrans.46.872.

13 D. Alders, L. Tjeng, F. Voogt, T. Hibma, G. Sawatzky, C. Chen, J. Vogel, M. Sacchi and S. Iacobucci, Temperature and thickness dependence of magnetic moments in NiO epitaxial films, *Phys. Rev. B: Condens. Matter Mater. Phys.*, 1998, **57**, 11623–11631, DOI: 10.1103/PhysRevB.57.11623.

14 S. Middey, J. Chakhalian, P. Mahadevan, J. W. Freeland, A. J. Millis and D. D. Sarma, Physics of ultrathin films and heterostructures of rare earth nickelates, *Annu. Rev. Mater. Res.*, 2016, **46**, 305–334, DOI: 10.1146/annurev-matsci-070115-032057.

15 P. S. Miedema, M. Beye, R. Könnecke, G. Schiwietz and A. Föhlisch, Thermal evolution of the band edges of 6H-SiC: X-ray methods compared to the optical band gap, *J. Electron Spectrosc. Relat. Phenom.*, 2014, **197**, 37–42, DOI: 10.1016/j.elspec.2014.08.003.

16 K. Kunnus, I. Josefsson, S. Schreck, W. Quevedo, P. S. Miedema, S. Techert, F. M. F. de Groot, A. Föhlisch, M. Odelius and P. Wernet, Quantifying covalent interactions with resonant inelastic soft X-ray scattering: case study of Ni^{2+} aqua complex, *Chem. Phys. Lett.*, 2017, **669**, 196–201, DOI: 10.1016/j.cplett.2016.12.046.

17 S. Schreck, A. Pietzsch, B. Kennedy, W. Quevedo, P. S. Miedema, C. Såthe, S. Techert, J. A. Terschlüsen, V. N. Strocov, T. Schmitt, F. Hennies, J.-E. Rubensson, P. Wernet and A. Föhlisch, Ground state potential energy surfaces around selected atoms from resonant inelastic X-ray scattering, *Sci. Rep.*, 2016, **6**, 20054, DOI: 10.1038/srep20054.

18 L. J. P. Ament, M. van Veenendaal, T. P. Devereaux, J. P. Hill and J. van den Brink, Resonant inelastic X-ray scattering studies of elementary excitations, *Rev. Mod. Phys.*, 2011, **83**, 705–767, DOI: 10.1103/RevModPhys.83.705.

19 F. J. Himpsel, Photon-in photon-out soft X-ray spectroscopy for materials science, *Phys. Status Solidi*, 2011, **248**, 292–298, DOI: 10.1002/pssb.201046212.

20 B. L. Henke, E. M. Gullikson and J. C. Davis, X-ray interactions: photoabsorption, scattering, transmission and

This journal is © the Owner Societies 2019

Phys. Chem. Chem. Phys., 2019, **21**, 21596–21602 | **21601**

reflection at E = 50–30 000 eV, Z = 1–92, *At. Data Nucl. Data Tables*, 1993, **54**, 181–342.

21 M. Beye and P. S. Miedema, Solid flexRIXS: A RIXS end-station for solid systems at BESSY II, *J. Large-Scale Res. Fac.*, 2017, **3**, A124.

22 G. Schiwietz, M. Beye and T. Kachel, UE112_PGM-1: an open-port low-energy beamline at the BESSY II undulator UE112, *J. Large-Scale Res. Facil. JLSRF.*, 2015, **1**, A33.

23 P. S. Miedema and M. Beye, Total 3s emission yield as bulk-sensitive probe for a true soft X-ray absorption spectrum?, *J. Phys. Chem. Lett.*, 2018, **9**, 2579–2583, DOI: 10.1021/acs.jpclett.8b00720.

24 M. W. Haverkort, G. Sangiovanni, P. Hansmann, A. Toschi, Y. Lu and S. Macke, Bands, resonances, edge singularities and excitons in core level spectroscopy investigated within the dynamical mean-field theory, *EPL*, 2014, **108**, 57004, DOI: 10.1209/0295-5075/108/57004.

25 M. W. Haverkort, M. Zwierzycki and O. K. Andersen, Multi-plet ligand-field theory using Wannier orbitals, *Phys. Rev. B: Condens. Matter Mater. Phys.*, 2012, **85**, 165113, DOI: 10.1103/PhysRevB.85.165113.

26 M. W. Haverkort, Quanty for core level spectroscopy - excitons, resonances and band excitations in time and frequency domain, *J. Phys.: Conf. Ser.*, 2016, **712**, 012001, DOI: 10.1088/1742-6596/712/1/012001.

27 P. S. Miedema, S. Stepanow, P. Gambardella and F. M. F. de Groot, 2p X-ray absorption of iron-phthalocyanine, *J. Phys.: Conf. Ser.*, 2009, **190**, 012143, DOI: 10.1088/1742-6596/190/1/012143.

28 F. de Groot and A. Kotani, *Core Level Spectroscopy of Solids*, CRC Press, 2008.

29 P. S. Miedema, R. Mitzner, S. Ganschow, A. Föhlisch and M. Beye, X-ray spectroscopy on the active ion in laser crystals, *Phys. Chem. Chem. Phys.*, 2017, **19**, 218000.

30 S. G. Chiuzbăian, G. Ghiringhelli, C. Dallera, M. Grioni, P. Amann, X. Wang, L. Braicovich and L. Patthey, Localized electronic excitations in NiO studied with resonant inelastic X-ray scattering at the Ni M threshold: Evidence of spin flip, *Phys. Rev. Lett.*, 2005, **95**, 197402, DOI: 10.1103/PhysRevLett.95.197402.

31 H. P. Rooksby, Structure of nickel oxide, *Nature*, 1943, **152**, 304.

32 A. Freitag, V. Staemmler, D. Cappus, C. A. Ventrice Jr., K. Al Shamery, H. Kuhlenbeck and H. J. Freund, Electronic sur-face states of NiO (100), *Chem. Phys. Lett.*, 1993, **210**, 10–14, DOI: 10.1016/0009-2614(93)89091-U.

33 F. Marschall, Z. Yin, J. Rehanek, M. Beye, F. Döring, K. Kubiček, D. Raiser, S. T. Veedu, J. Buck, A. Rothkirch, B. Rösner, V. A. Guzenko, J. Viefhaus, C. David and S. Techert, Transmission zone plates as analyzers for effi-cient parallel 2D RIXS-mapping, *Sci. Rep.*, 2017, **7**, 8849, DOI: 10.1038/s41598-017-09052-0.

34 Z. Yin, H. Löchel, J. Rehanek, C. Goy, A. Kalinin, A. Schottelius, F. Trinter, P. Miedema, A. Jain, J. Valerio, P. Busse, F. Lehmkühler, J. Möller, G. Grübel, A. Madsen, J. Viefhaus, R. E. Grisenti, M. Beye, A. Erko and S. Techert, X-ray spectro-scopy with variable line spacing based on reflection zone plate optics, *Opt. Lett.*, 2018, **43**, 4390–4393.